ADVANCED FUNCTIONAL MATERIALS
www.afm-journal.de

Crosslinking-Modulated Hydrogel Piezoionic Senor for Pattern Security Authentication in Human-Machine Interfaces

Yue Sun, Guo Tian, Tao Yang, Shenglong Wang, Boling Lan, Xuelan Li, Tianpei Xu, Long Jin, Weili Deng, and Weiqing Yang**

Ionic hydrogels are uniquely suited as force-sensing layers because of their good biocompatibility and controlled electromechanical properties. The emerging piezoionic effect allows them to sense the position of pressure, but the low response rate limits their applications. Herein, this work focuses on modulating the response time of piezoionic outputs through crosslinking. The underlying mechanism is investigated through the perspective of deformation recovery rate and ion migration behavior in the ionic hydrogels. As a result, the developed piezoionic sensors are capable of distinguishing static forces in the range of 0.1–5 s while monitoring dynamic force, breaking the limitations of conventional self-powered pressure sensors that have trouble tracking static forces. Furthermore, by utilizing the piezoionic effect to convert the touch indentation into transverse gradient ionic potential, the constructed piezoionic sensors achieve accurate monitoring of finger pressing position and sliding trajectory. As a proof-of-concept, pattern unlocking in security authentication is successfully validated based on the developed piezoionic sensors. This design strategy of modulating ionic tactile sensor by crosslinking is expected to provide a fresh path for the large-scale flexible human-machine interfaces.

1. Introduction

The growing human-machine interactions have driven up the significance of tactile sensing in human-machine interfaces (HMI).[1–7] At present, pressure sensing modules for wearable devices and robot surfaces are still dominated by rigid materials, limiting their application scenarios and scope.[8–11] Flexible force sensing materials have emerged one after another to enhance HMI compatibility, improving the conformal adhesion between devices and the human body, and alleviating the signal distortion caused by mismatched interfaces in conventional sensors.[12–23] Among them, ionic hydrogels are commonly used in force-sensitive layers of wearable devices due to their biocompatibility, adhesion, bio-like ionic conductive mechanisms, and tunable mechanical properties.[24–31] Conventionally, achieving an accurate perception of external pressure information over a large area usually requires the integration of several sensor arrays, with significant challenges in device encapsulation and wiring.[32,33] In particular, the high viscoelasticity associated with water content makes hydrogel-based sensors more challenging to integrate, miniaturize, and array.[34–36] Therefore, researchers present an ionic hydrogel touch panel that can detect force-related information using changes in capacitance, thus simplifying the requirements of sensor integration.[28] Even so, the issue of powering capacitive touch panels still limits their applications in HMI.

The piezoionic effect, a novel force-sensitive sensing mechanism, has gradually gained more attention in recent years.[37–39] It describes the ion current produced by the potential difference due to the imbalance of internal ion charges when a pressure gradient exists. The difference in local dynamic migration of ions is a main feature that distinguishes the piezoionic effect from other electromechanical sensing mechanisms. With this feature, it is possible to monitor the magnitude and position of the force simultaneously.[40–44] It has been reported that in the polyelectrolyte polyacrylic acid hydrogel system, the distribution gradient between the positively charged hydrogen ion and the negative charge of the fixed chain after compression provides an opportunity for electromechanical conversion and recycle sensing, so as to develop self-powered position recognizers.[42] Also as a self-powered sensing mechanism, piezoionic sensing is better suited than piezoelectric sensing to work in humid environments with sweat or body fluids and to monitor low-frequency dynamic or static forces.[30,39] According to the aforementioned research, regardless of whether the devices are employed for energy harvesting or sensing, the design of piezoionic devices tends to focus

Y. Sun, G. Tian, T. Yang, S. Wang, B. Lan, X. Li, T. Xu, L. Jin, W. Deng, W. Yang
Key Laboratory of Advance Technologies of Materials
School of Materials Science and Engineering
Southwest Jiaotong University
Chengdu 610031, P. R. China
E-mail: weili1812@swjtu.edu.cn; wqyang@swjtu.edu.cn
W. Yang
Research Institute of Frontier Science
Southwest Jiaotong University
Chengdu 610031, P. R. China

The ORCID identification number(s) for the author(s) of this article can be found under https://doi.org/10.1002/adfm.202420187

DOI: 10.1002/adfm.202420187

on the unequal distribution of ions in the longitudinal direction parallel to the stress direction.[42,45–49] These designs overlooked the more interesting opportunities provided by horizontal ion migration that can take fully use of ion transfer in a single thin-film sensor.[50] Recently, an electrochemical luminous skin has been reported to convert external stimuli into visual luminescent signals without a spatially distributed sensor array, taking advantage of the property that ions move only in the vicinity of the indentation zone in the viscoelastic matrix.[51] Inspired by this, a single hydrogel can generate multiple pressure gradients due to the transverse migration of ions in the matrix, thus promising multi-point sensing, whereas a single device of a traditional sensor can only correspond to one information point.[52] However, the response time of the piezoionic signal is significantly slower than that of other sensing mechanisms because of the viscoelasticity of the hydrogel matrix and the slower ion migration rate. To broaden the frequency range of the response and application scenarios, the response time of the piezoionic signal needs to be further optimized. The effects of polymer content, ion concentration, ion size, and hydrogel thickness on the response time of the pressure ionization signal were discussed in previous studies (Figure S1, Supporting Information).[37] Given the significant effect of polymer gap size on ion migration, a thorough discussion of the impact of polymer crosslinking degree on response time is warranted, so as to seek guidance on regulating response time.

Herein, we revealed the regulation mechanism of the response time of the piezoionic signal by studying the influence of the crosslinking degree on the electromechanical coupling properties of hydrogels from the perspective of deformation recovery and ion migration recovery. Next, the fundamental reason why piezoionic sensors are capable of providing continuous, short-term static force monitoring is clarified by an analysis of the piezoionic signal generation. On this basis, a single piezoionic hydrogel sensor enables the accurate and rapid monitoring of pressure position and trajectory. This work clarifies the possibility and advantages of the piezoionic effect in the field of pressure acquisition and offers an innovative direction for the practical application of hydrogels in flexible HMI.

2. Results and Discussion

2.1. Biomimetic Tactile Perception of Ionic Hydrogel Based on Piezoionic Effect

Ionic hydrogels can serve as the bionic skin for robots or prosthetic limbs instead of conventionally stiff materials. As depicted in **Figure 1**a, the piezoionic effect enables the ionic hydrogels to perform sensing functions like force monitoring and trajectory recognition, thereby facilitating the security authentication of intelligent systems in HMI. Typically, human skin receptors convert the tactile sensation into electrophysiological signals, which are then transmitted via ion conduction to the brain for processing and interpretation.[40] As illustrated in Figure 1b, ionic hydrogels have the similar characteristics of electric signal transmission through ion transfer to human skin.[53,54] When a force is applied to an ionic hydrogel, it turns into a potential difference due to the imbalance of positive and negative ions in the hydrogel network. Thus, the pressure information at different positions can be obtained within a single thin film, similar to the tactile sensation of human skin, without the necessity for multi-unit integration. In addition, the advantages of ionic hydrogels, such as being transparent, biocompatible, and conformal, make them irreplaceable in the construction of tactile sensors. Figure 1c shows that the prepared ionic hydrogel fits perfectly on the skin. On this basis, pressure information can be obtained by measuring the potential difference at various points, which can then be integrated with machine learning to provide more accurate pressure distribution information. When the finger presses the hydrogel, the space of the polymer network at the pressing point becomes smaller, and the ions are driven by the interstitial water to move to the non-pressing zone (Figure 1d). The difference in the migration speed of positive and negative ions leads to the potential difference between the pressing point and the non-pressing zone, resulting in potential ΔV_{OA} and current ΔI_{OA}. Figure 1e shows the peak shape of the piezoionic signal, indicating that the response time of the piezoionic signal needs further optimization to adapt to more application scenarios.

2.2. Regulation of Ionic Hydrogel Crosslinking Degree on Signal Response Time

To improve the responsiveness of ionic hydrogel, we selected polyacrylamide (PAM) as the polymer skeleton, sodium chloride (NaCl) as the ionic electrolyte, and only controlled the addition of N,N′-Methylenebisacrylamide (MBAA) as crosslinker to carry out the following investigation. The prepared ionic hydrogel displays good transparency (**Figure 2**a), excellent mechanical performance (Figure S2, Supporting Information) and good universal adhesion (Figure S3, Supporting Information) due to the high content of water and dense polymer network. The rich water content provides the migration medium for ions, while the 3D porous network structure of the PAM provides mechanical support for the hydrogel. From the X-Ray Diffraction (XRD) spectra in Figure 2b, the pure PAM hydrogel only has a bulging peak at 23°, whereas the NaCl/PAM (1.5 M) hydrogel has not only a bulging peak at the same position but also distinctive peaks at 32°, 45°, 56°, 66°, and 75°, which are in agreement with the XRD standard card of the NaCl crystals (PDF-#88-2300).[55] These observations reveal that NaCl exists as crystals after water evaporation without forming chemical interactions with the polymer matrix, and it can be inferred that NaCl remains ions in the hydrogel, which provides the basis for electrical signal conduction. Under the same strain, the response time of piezoionic signal mainly depends on the ion migration rate, while the signal recovery time is affected by both the ion migration rate and the material deformation recovery rate. Therefore, this work mainly focuses on the responsiveness of the hydrogel matrices from the perspective of deformation and ion migration behavior. As illustrated in Figure 2c, a high crosslinking degree of the hydrogel results in narrower channels for ions to migrate through the polymer network, leading to a decrease in the total ion migration rate. However, the high cross-linked hydrogel recovers faster after the force is released because of the higher modulus of the material. This indicates that the higher the crosslinking degree, the slower ion migration and the faster the deformation recovery, while the opposite is true for hydrogels with low a crosslinking degree.

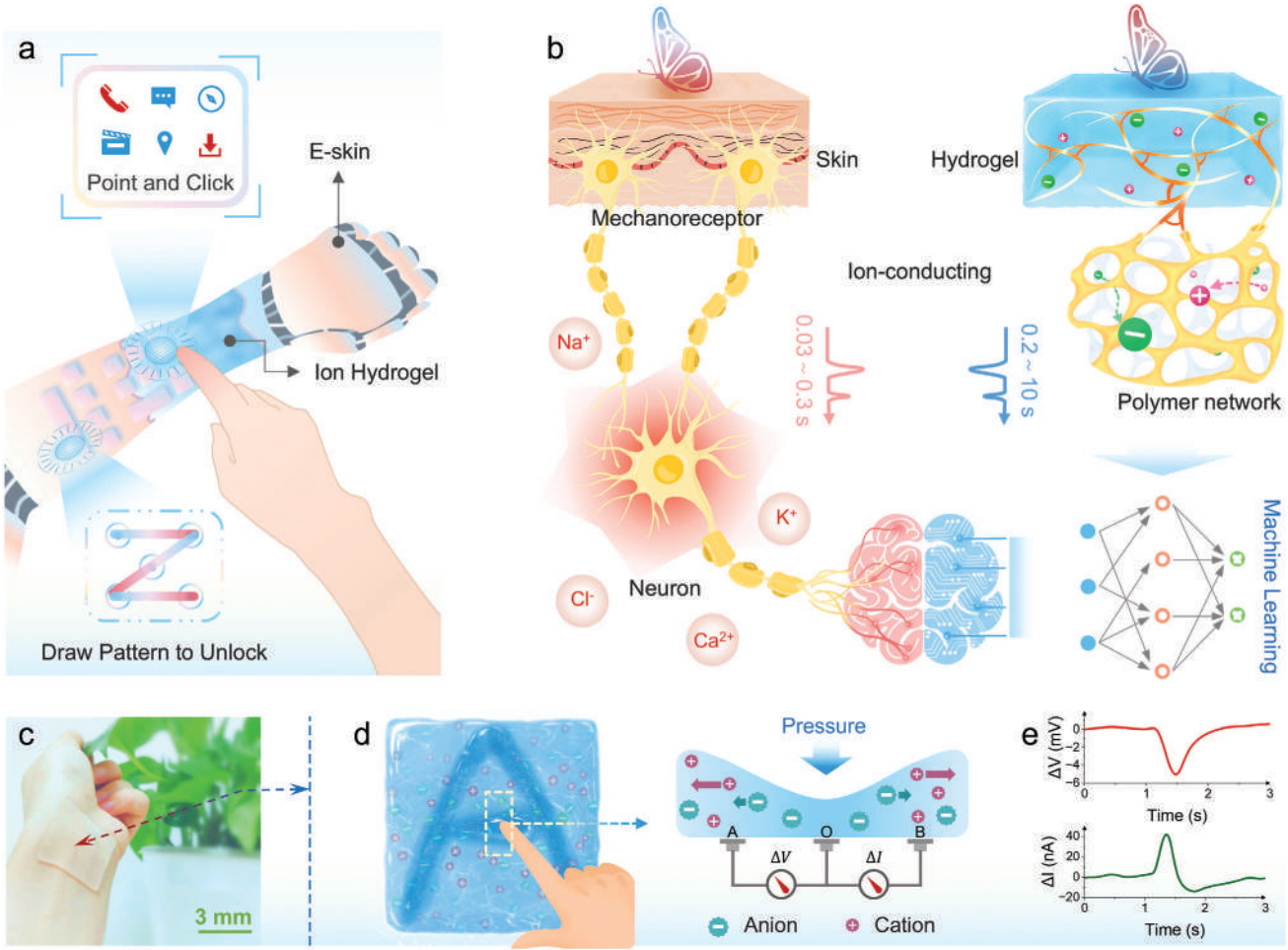

Figure 1. Diagram of force sensing based on ionic hydrogel in HMI. a) Ionic hydrogel for security authentication in human-machine interaction. b) Force conversion and electrical signal transmission in ionic hydrogel simulating human tactile perception. c) Photo of transparent ionic hydrogel. d,e) Piezoionic effect and piezoionic signal respons.

Therefore, the modulation of response speed is expected to be achieved by modulating the crosslinking degree of the hydrogel.

Based on the above reasoning, the NaCl/PAM ionic hydrogels with different contents of crosslinker (0.15‰, 0.75‰, 1.5‰, and 2.25‰ wt/wt), were prepared to investigate the effect of crosslinking degree on the properties. As shown in Figure 2d, the infrared spectra of hydrogel with different amounts of crosslinker show that the infrared absorption peaks at 1680 and 1617 cm^{-1} are also slightly enhanced with the increase in the content of crosslinker (MBAA) containing amide bonds. The differential scanning calorimetry (DSC) and Thermo-Gravimetric Analysis (TGA) curves show that melting temperature and peak intensity of PAM decrease and the peak width increases with the increase of crosslinker (Figure S4, Supporting Information). It is speculated that the crosslinking degree reduces the activity of the molecular chain and lowers the crystallinity. According to Figure 2e, the hydrogel with higher crosslinking degree can accommodate more interstitial water, which also affects the deformation recovery of the hydrogel. The results of swelling experiments show that the higher the crosslinker content, the sooner the swelling equilibrium is established (Figure 2f; Table S1, Supporting Information). The swelling degree of the hydrogel tends to be the same when the crosslinker content is ≈1.5‰ wt/wt, further indicating that the crosslinking degree of PAM is close to saturation (Figure 2g). Furthermore, the 2D small-angle X-ray scattering (SAXS) illustrates the change of crosslinking density on the molecular chain scale. It can be found that the radius of the diffraction ring becomes smaller and the point distribution becomes more concentrated with increasing crosslinker content (Figure 2h), which implies that the spaces within the crosslinked network become smaller.[56] The mechanical test was selected to ascertain the impact of crosslinking degree on the deformation recovery speed of ionic hydrogel. The compression modulus of ionic hydrogel increases with the crosslinking degree, and its internal drive to recover after stress is stronger, which is conducive to improving the response rate. At the same time, the compression modulus and compression cycle stability are also improved, while the elongation at break decreases (Figure 2i–k; Figure S5, Supporting Information). Apparently, the increase in crosslinking degree can enhance the modulus of hydrogel, improve the rebound speed, and reduce the plastic deformation. In addition, experimental analysis was conducted to investigate the effect of

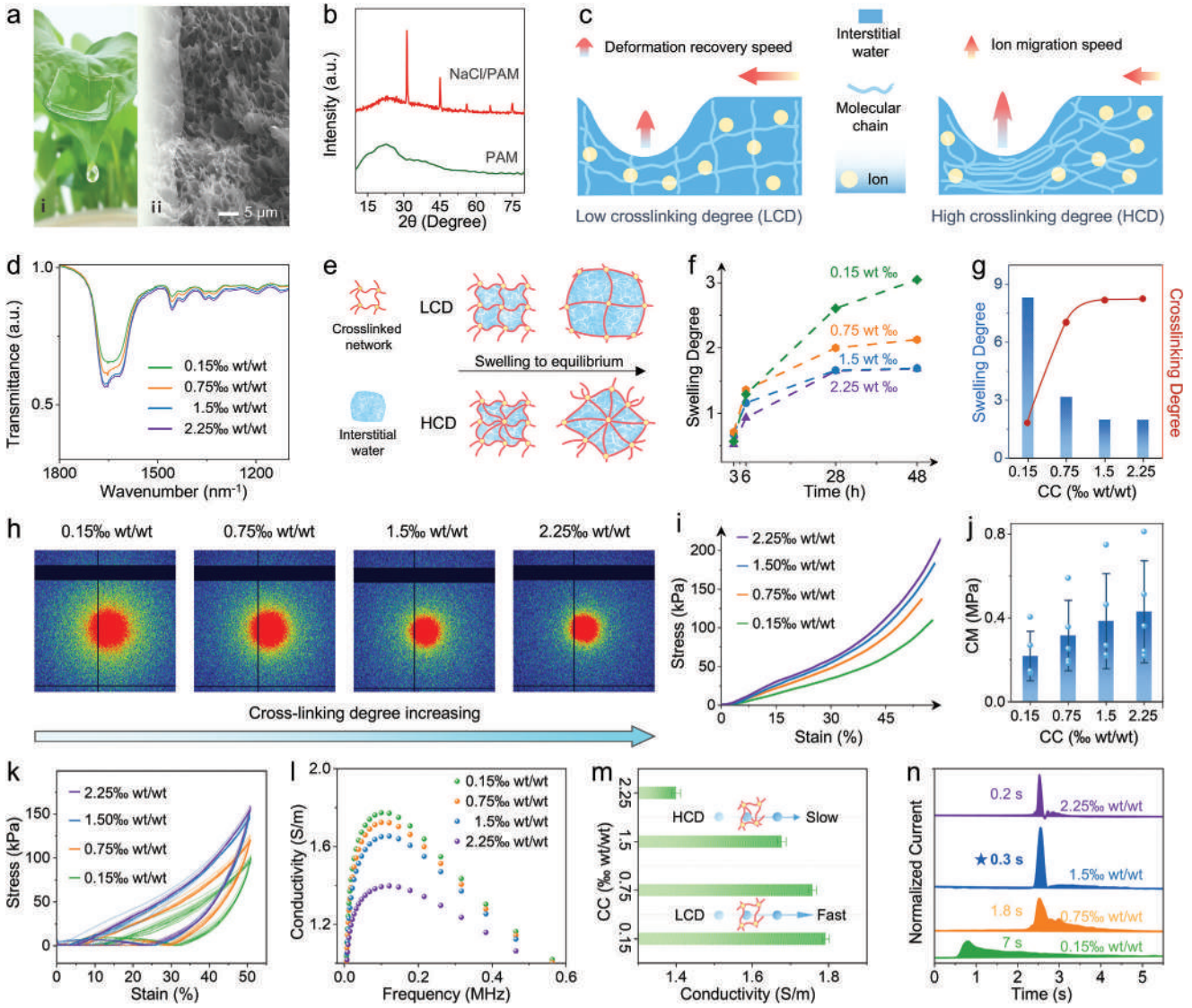

Figure 2. Regulation of crosslinking degree on the piezoionic responses in ionic hydrogels. a) Picture and SEM microscopic morphology of transparent ionic hydrogel. b) XRD spectra of pure PAM hydrogel and NaCl/PAM hydrogel after freeze drying. c) Schematic diagram of the influence of crosslinking degree on deformation recovery speed and ion migration rate, the longer the arrow, the faster the speed. d) FTIR spectrum of hydrogel with different contents of crosslinker. e) Schematic diagram of the relationship between crosslinking degree and swelling degree. f) Swelling degree of hydrogel with different contents of crosslinker. g) The swelling degree and relative crosslinking degree after reaching swelling equilibrium (results after 1 week), crosslinker content (CC). h) 2D SAXS diffraction patterns of hydrogels with different crosslinker contents. i) Compressive stress-strain curve, j) compressive modulus (CM), and k) compression cyclic stress-strain curves of hydrogels with different contents of crosslinker. l) Frequency-responsive ion conductivity. m) Ion conductivity. n) Response time of piezoionic signals.

crosslinking degree on ion migration rate. It is evident that the ion conductivity of the frequency response decreases with increasing the crosslinking degree (Figure 2l). Consistently, the results calculated from the impedance spectrum also confirm this law (Figure 2m). The ion conductivity decreases sharply with a crosslinker of 2.25‰ wt/wt, probably due to the small pore size in the polymer network, which seriously hinders the migration of solvation ions.[57] In Figure 2n, the more crosslinker, the shorter the signal response and recovery time. Nevertheless, when the crosslinker is 2.25‰ wt/wt, the signal strength decreases under the same strain. This phenomenon can be explained by the too-tiny pore size of crosslinked network, which reduces the ion migration rate, resulting in a fall in the piezoionic output. Based on the above, the ionic hydrogel system with a crosslinker of 1.5‰ wt/wt was used for the subsequent experiments.

2.3. The mechanism and Pressure Sensing Performance of Piezoionic Sensors for Position Detection

To better understand the ability of ionic hydrogel to perceive the magnitude and position of forces, we intercepted the output of the piezoionic signal during a pressing cycle as an example. As shown in **Figure 3**a, there is no signal output in the initial state,

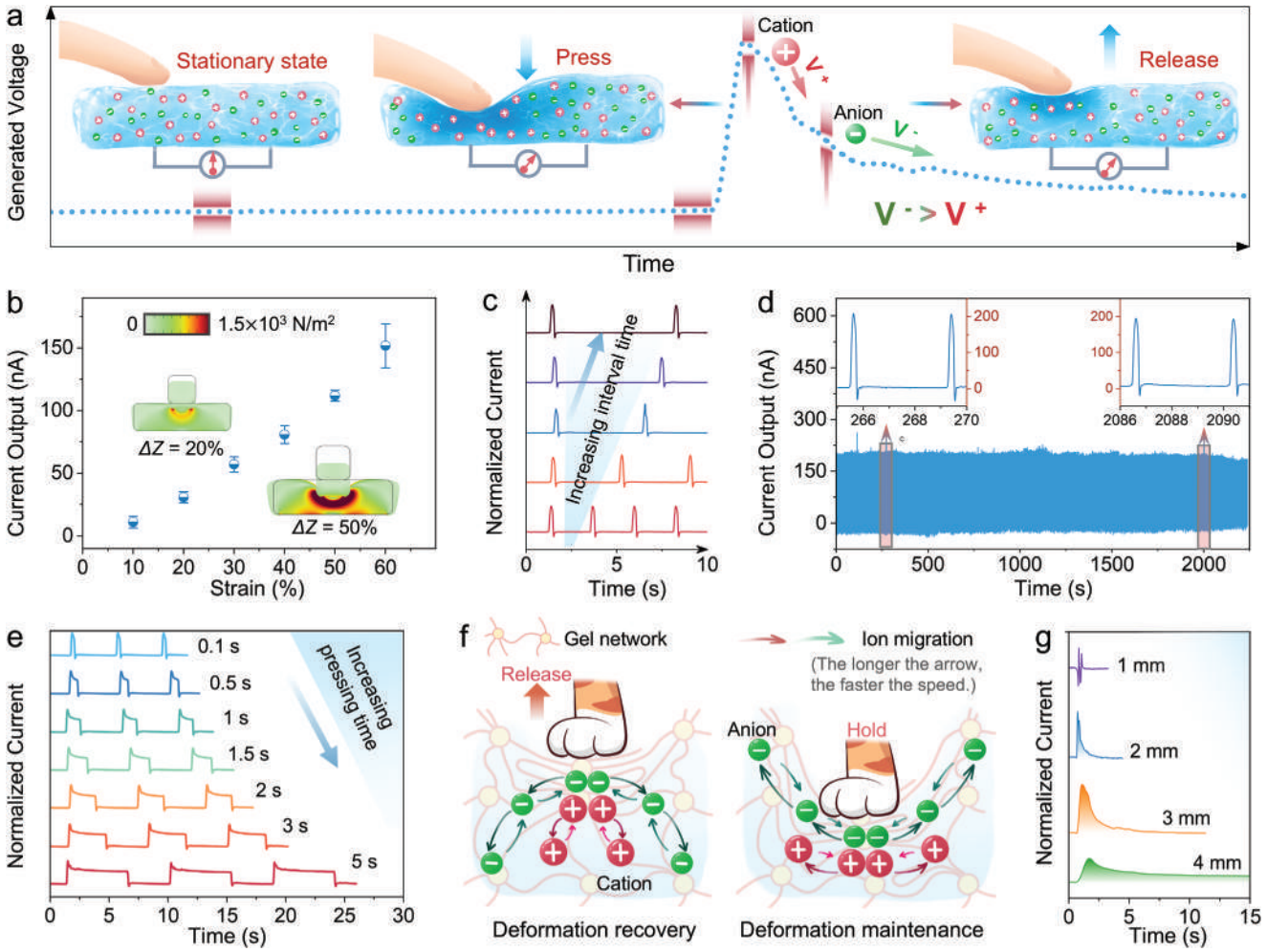

Figure 3. Piezoionic sensing mechanism and electromechanical sensing performance of ionic hydrogels. a) Ion migration behavior and electrical signal state corresponding to the pressing state. b) Electrical signals corresponding to the pressing state and simulation diagram of internal pressure of the deformed hydrogel. c) Piezoionic outputs with increased pressing interval time. d) Stability test of piezoionic sensor with compression cycling. e) Piezoionic outputs with increased holding time. f) Ion migration behavior under deformation recovery and deformation holding. g) Piezoionic outputs of sensors with different hydrogelthicknesses.

and the positive and negative ions are evenly dispersed throughout the hydrogel. As the finger presses, the pressure drives the solvation ions in the indentation zone to migrate with the interstitial water to the non-indentation zone, where the network space is larger (Figure S6, Supporting Information). In light of the size filtering and flow resistance effects of the polymer network, the migration rate of chloride ions with smaller solvation ion size is faster than that of sodium ions.[37,58] Within a thin layer, the ions move laterally in the hydrogel film under pressure. The potential difference at various locations on the surface of hydrogel will be established as the displacement difference between positive and negative ions rises. The electrodes on the same side of hydrogel can monitor the piezoionic signals from the non-indented zone and the indented zone (Figure S7, Supporting Information).

To gain insight into the potential application of piezoionic sensors in HMI, the pressure sensing performance of individual devices was characterized and analyzed. As shown in Figure 3b, the generated current signal and strain are almost linearly correlated within the strain range of 10%–60%. According to the simulation results of the pressure distribution in viscoelastic materials during indentation testing, it can be found that the pressure presents a gradient distribution extending outward from the core location, with pressure dropping as distance increases (Figure S8, Supporting Information). It further indicates that the pressure distribution of the material, as well as the relative positions of the electrode and the indentation, are strongly correlated with the strength of the piezoionic signal. Meanwhile, within the range of 15–75 kPa, the piezoionic sensor maintains good linearity and sensitivity (Figure S9, Supporting Information). When the pressure exceeds 75 kPa, the piezoionic sensitivity drops sharply due to the nonlinear relationship between pressure and water flux in the cross-linked network. Additionally, the device captured dynamic pressures precisely at various frequencies (Figure 3c). And there is no loss of signals at different frequencies, indicating that the signal response time at this crosslinking degree can meet the pressure monitoring needs of a wider frequency range. After

continuous testing at 60% strain for 500 cycles, the signal remains almost unchanged (Figure 3d), suggesting that the piezoionic sensor has good fatigue resistance and cycle stability. Referring to Figure S10 (Supporting Information), comparison of the electromechanical performance of the ionic hydrogel before and after 7 days shows that the piezoionic sensors have good performance stability under sealed conditions.

In addition to monitoring the dynamic pressure, it is surprising to find the possibility of the ionic hydrogel piezoionic sensorsin static pressure monitoring. The slow recovery of the pressure ionization signal implies that the ions are slow to reestablish potential balance in the compressed crosslinked network if the hydrogel is not released after pressing. To verify this hypothesis, the hydrogel was pressed to 60% of the strain and kept still. The piezoionic signals slowly fall back during the strain holding period (Figure 3e). After the pressure is released, the signals return to the baseline, and the static pressure monitoring in this experiment can clearly record the holding time from 0.5 to 5 s. This possible intrinsic mechanism of this static force monitoring is illustrated in Figure 3f. When the applied force is withdrawn immediately, positive and negative ions migrate through the polymer network with the assistance of deformation recovery and potential difference, resulting in rapid charge balance. However, if the force is held, the molecular network space at the indentation is extremely small, which limits the migration of solvation ions. Meanwhile, without the drive of elastic recovery, the speed at which ions establish charge balance is further delayed, resulting in temporary ion potential retention.

In addition, we further explored the effect of different thicknesses of ionic hydrogels on the output signal at the same indentation depth to obtain a faster response time for the piezoionic sensor. As shown in Figure 3g, ionic hydrogel is too thin and low in ions, resulting in a fast signal response but low signal intensity. In the other case, ionic hydrogel is too thick with the pressure dispersed over a larger range (Figure S11, Supporting Information), resulting in a slow signal response and low signal intensity. After a thorough weighing, the ionic hydrogel with a thickness of 2 mm was chosen for application verification in further trials. Moreover, the concentration of NaCl also significantly affects the electrical output. The higher the concentration, the stronger the signal output, exceeding 2 M, the output decreases (Figure S12, Supporting Information). In summary, the developed ionic hydrogel based on piezoionic effect can monitor dynamic and static pressure simultaneously, demonstrating great potential in the field of human-machine interaction.

2.4. Security Authentication of Ionic Hydrogel Sensor for Pattern Unlocking

After understanding the piezoionic sensing mechanism of ionic hydrogels, a force sensor was designed, as shown in **Figure 4a**. Multiple electrodes were integrated on a single hydrogel film to track the position and trajectory of the pressure within the electrode coverage. Taking the pressing positions of center points O as an example, as shown in Figure 4b, when pressing point O, the indentation forms a negative ion charge retention zone at the center and a positive charge migration zone around it. Therefore, all four channels have negative potential (V_{OA}, V_{OB}, V_{OC}, and V_{OD}) and consistent signal strength. Similarly, when pressing point A, the positive charge migrates outward from the center of the indentation, and other channels are not within the radiation range of the indentation. So, only the OA channel generates a positive potential. To further ascertain the related pressure trajectory, we summarized the location signal pattern of single-point pressure and observed the output signal of each channel (Figure 4c). When pressing the point O, the OA channel displays a negative potential initially, followed by a positive potential, while other channels only generate negative potentials, as shown in signal group **i**. In contrast, the output of indentation sliding is represented by signal group **ii**. Analogous analysis can deduce that the signal group **ii** is the output of the sensor sliding from point A to point O. Thus, the trajectory of the press can be determined by these signals.

Given its function in force position detection, coupled with the ion conduction mechanism, excellent mechanical properties, and biocompatibility of the sensitive layer, the designed piezoionic sensor has unique advantages in the field of pressure sensing in HMI. To verify and unleash the potential of the piezoionic sensor, the experiment further tested its feasibility for safety authentication. As presented in Figure 4d, after presetting the pattern password, manually touching and sliding the unlock pattern can realize the security authentication. After the piezoionic hydrogel converts the indentation into electric outputs, the peak shape and time of occurrence of the four-channel signal can determine the sequence of which points the finger pressed and slid over, and thus infer the input pattern. In this way, the system can determine if the input pattern is valid. This work simply shows how to unlock the most basic patterns. More complicated patterns can be accurately monitored and replicated in the future by integrating machine learning, multi-electrode array distribution, and static pressure monitoring. More importantly, the traditional integrated array sensor requires five single sensors, including ten electrodes connected to ten wires, and a complex integrated packaging to enable path recognition. While the developed piezoionic sensor only requires one sensitive layer and five electrodes connected to five wires to realize the same function. Its single sensitive layer and more simplified wiring introduce a new path for spatially distributed high-resolution sensors, with significant advantages and possibilities in the fields of flexible touch screens and HMI.

3. Conclusion

In summary, this work focused on the response time regulation of the hydrogel piezoionic sensor. From the perspective of polymer crosslinking degree, the effect of crosslinker content on the electromechanical properties of the hydrogel was studied in terms of deformation recovery and ion migration of the hydrogel. After deeply analyzing the piezoionic sensing mechanism and optimizing the responsiveness of ionic hydrogel, the developed piezoionic sensor exhibited good linearity (strain range of 10%–60%) and stability (500 cycles). Meanwhile, it was surprisingly discovered that the piezoionic sensors can monitor short-term static force (0.1 to 5 s) while monitoring dynamic force processes, further enriching its prospects in the field of tactile sensing. Based on the uneven local distribution of ions near the indentation, the single ionic hydrogel pressure sensor realized

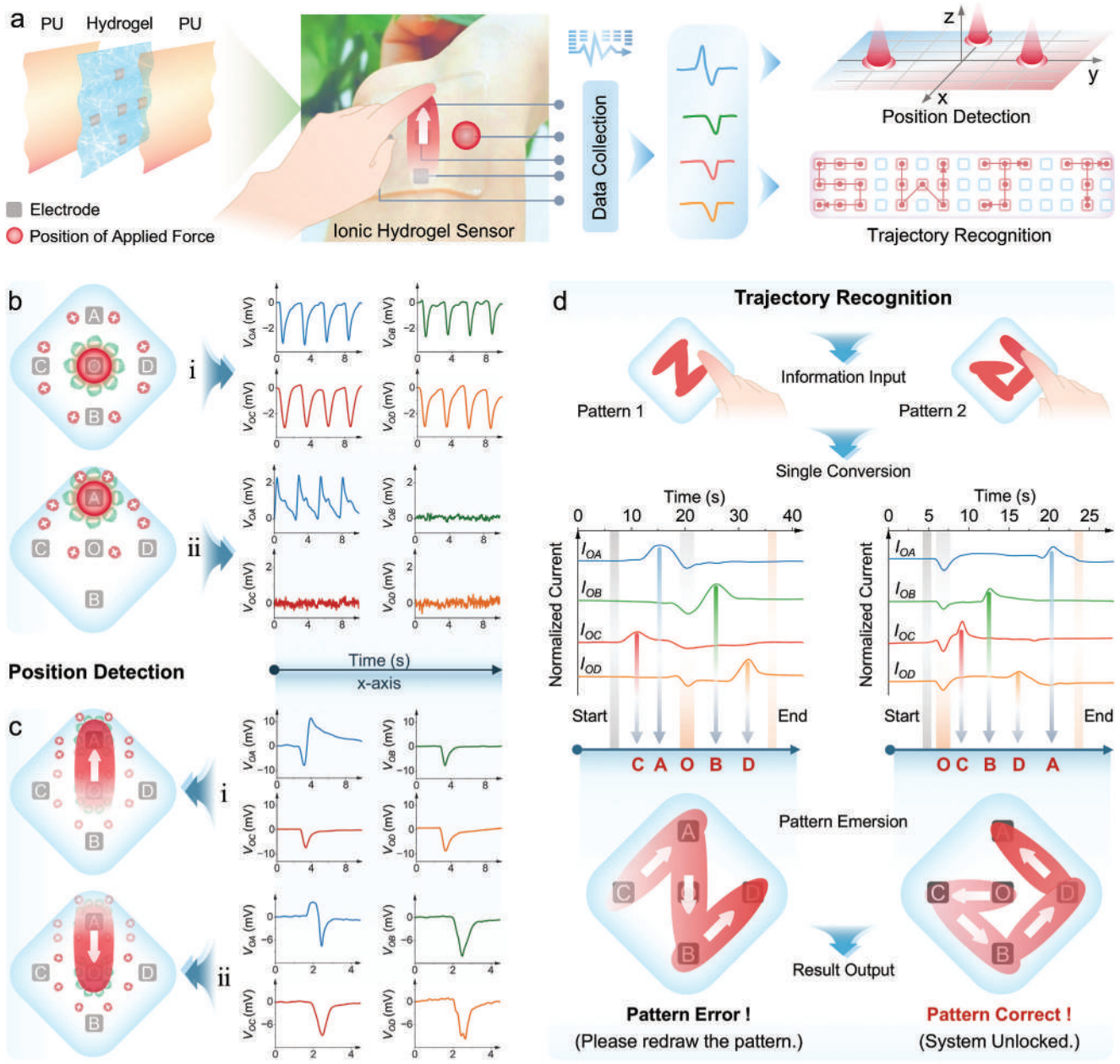

Figure 4. Ionic hydrogel piezoionic sensors for security authentication. a) Structure, signal acquisition, and data processing of piezoionic sensors for position detection and trajectory recognition. b) Single-point position detection. c) Sliding trajectory detection. d) Pressure trajectory recognition for pattern unlocking.

force trajectories identification and was successfully used for pattern unlocking safety authentication. Consequently, it is expected that this crosslinking-modulated hydrogel piezoionic sensor design will significantly simplify device manufacturing and provide a more reliable way for HMI and e-skin research.

4. Experimental Section

Preparation of Ionic Hydrogels with Different Crosslinking Degree: In 20 mL of deionized water, add 1.75 g of NaCl with 6.67 g of acrylamide (AM), and stir for 15 min. Subsequently, incorporate 0.01 g of MBAA (Aladdin, AR) and 250 µL of 20 wt.% sodium persulfate (APS, Aladdin, AR) solution into the previously mentioned mixture, and mix for a duration of 30 min. Place the fully stirred solution in the refrigerator for 30 min. In the fume hood, add 20 µL of N, N, N', N'-Tetramethylethylenediamine (TEMED, Aladdin, AR) to the cooled solution. Shake it up rapidly, then pour the solution into a polytetrafluoroethylene (PTFE) mold, cover it with a glass sheet, and left for 6 h to transform into hydrogel. After demolding, the surface was cleaned and dried with deionized water to obtain ionic hydrogel. The pure hydrogel was obtained without adding NaCl. Different amounts of the crosslinker MBAA (0.15‰, 0.75‰, 1.5‰ and 2.25‰ wt/wt, respectively) were used to prepare the ionic hydrogels with varying degrees of crosslinking.

Fabrication of Ionic Hydrogel Piezoionic Sensor: The device consists of a sensing functional layer, electrodes, wires, and packaging layer. The sensing functional layer is an ionic hydrogel with a size of 20 mm × 20 mm × 2 mm. When studying the influence of thickness on response time, the hydrogels with a thickness of 1 mm, 2 mm, 3 mm, and 4 mm were simultaneously prepared. The electrode is a carbon cloth with a size of 3 mm × 3 mm. Wrap the copper wire with double-layer carbon cloth as the electrode and fix it on the hydrogel. The distance between the two electrodes on the same side is 1 cm. Finally, the piezoionic sensor component was obtained by encapsulating it with commercial polyurethane film. The distance between the electrodes of the device used for position detection and trajectory recognition is 5 mm.

Characterization and Measurement—Materials Section: The microscopic morphology images were characterized by scanning electron microscopy (SEM, JSM-7800F) with an accelerating voltage of 5 kV. The XRD diffraction (Empyrean, PANalytical) and Fourier transform infrared spectroscopy (FTIR; Nicolet iS50) in attenuated total reflectance (ATR) mode were applied to study the composition of ionic hydrogels. The thermal stability of hydrogels was investigated by DSC (Waters; heating rate, 5 °C min^{-1}) and TGA/DSC3+ (Mettler Toledo; heating rate, 10 °C min^{-1}). Samples for adhesion testing were pulled at 5 mm min^{-1} using a universal testing machine (UTM, Instron 5567, USA) until the samples were separated from the substrate. Rotational rheometer (TA DHR-1, USA) and SAXS (Xeuss 3.0) were used to characterize the network crosslinking degree of the hydrogels. The frequency-dependent curve data of ion conductivity was measured by an electrochemical workstation (CH Instruments, CHI660E). The data measured by UTM was used to analyze the influence of crosslinking degree on the mechanical properties of ionic hydrogels. The stretching sample size is 50 mm × 8.5 mm × 2 mm, the stretching test speed is 10 mm min^{-1}, the compression sample size is 20 mm × 20 mm × 5 mm, and the compression test speed is 5 mm min^{-1}. The swelling ratio and swelling degree were tested under the same conditions, and the hydrogels were cut into blocks and placed in water for standing at the same time. Take out the hydrogel at the same interval and dry the surface water before weighing.

Characterization and Measurement—Device Section: To investigate the piezoionic performance, a linear motor (LinMotH01-23×86/160) with a force gauge (IMADA model ZPS-DPU-50 N) was used to apply pressure to the device, and the resulting current and voltage output signals were monitored via a programmable electrometer (Keithley 6514). The force for position determination and trajectory recognition was applied by finger pressing and sliding.

Supporting Information

Supporting Information is available from the Wiley Online Library or from the author.

Acknowledgements

W.D. acknowledges the National Natural Science Foundation of China (No. U2330120), the Natural Science Foundation of Sichuan Province of China (No. 2023NSFSC0313), and the Basic Research Cultivation Project of Southwest Jiaotong University (No. 2682023KJ024). Thanks for the help from the Analysis and Testing Center of Southwest Jiaotong University.

Conflict of Interest

The authors declare no conflict of interest.

Author Contributions

Y.S. performed conceptualization methodology, investigation, and formal analysis, and wrote. G.T. performed conceptualization methodology and investigation. T.Y. performed conceptualization methodology and investigation. S.W. performed conceptualization methodology and formal analysis. B.L. performed conceptualization methodology and formal analysis. X.L. performed conceptualization methodology and formal analysis. T.X. performed conceptualization methodology and investigation. L.J. performed conceptualization methodology and investigation. W.D. performed conceptualization methodology, investigation, and formal analysis, and wrote. W.Y. performed conceptualization methodology, supervision, resources, project administration, funding acquisition, and wrote.

Data Availability Statement

The data that support the findings of this study are available from the corresponding author upon reasonable request.

Keywords

crosslinking degree, human-machine interfaces, piezoionic effect, response time, tactile sensor

Received: October 23, 2024
Revised: December 17, 2024
Published online:

[1] B. Zhang, J. Li, J. Zhou, L. Chow, G. Zhao, Y. Huang, Z. Ma, Q. Zhang, Y. Yang, C. K. Yiu, J. Li, F. Chun, X. Huang, Y. Gao, P. Wu, S. Jia, H. Li, D. Li, Y. Liu, K. Yao, R. Shi, Z. Chen, B. L. Khoo, W. Yang, F. Wang, Z. Zheng, Z. Wang, X. Yu, *Nature.* **2024**, *628*, 84.
[2] H. Lu, Y. Zhang, M. Zhu, S. Li, H. Liang, P. Bi, S. Wang, H. Wang, L. Gan, X.-E. Wu, Y. Zhang, *Nat. Commun.* **2024**, *15*, 3289.
[3] J. Yin, S. Wang, T. Tat, J. Chen, *Nat. Rev. Bioeng.* **2024**, *2*, 541.
[4] N. Li, Z. Wang, X. Yang, Z. Zhang, W. Zhang, S. Sang, H. Zhang, *Adv. Funct. Mater.* **2024**, *34*, 2314419.
[5] Y. Park, H. Luan, K. Kwon, T. S. Chung, S. Oh, J.-Y. Yoo, G. Chung, J. Kim, S. Kim, S. S. Kwak, J. Choi, H.-P. Phan, S. Yoo, H. Jeong, J. Shin, S. M. Won, H. J. Yoon, Y. H. Jung, J. A. Rogers, *npj Flex. Electron.* **2024**, *8*, 6.
[6] Z. Cao, Y. Xu, S. Yu, Z. Huang, Y. Hu, W. Lin, H. Wang, Y. Luo, Y. Zheng, Z. Chen, Q. Liao, X. Liao, *Adv. Funct. Mater.* **2024**, https://doi.org/10.1002/adfm.202412649.
[7] Z. Huang, S. Yu, Y. Xu, Z. Cao, J. Zhang, Z. Guo, T. Wu, Q. Liao, Y. Zheng, Z. Chen, X. Liao, *Adv. Mater.* **2024**, *36*, 2407329.
[8] Y. Jiang, S. Ji, J. Sun, J. Huang, Y. Li, G. Zou, T. Salim, C. Wang, W. Li, H. Jin, J. Xu, S. Wang, T. Lei, X. Yan, W. Y. X. Peh, S. C. Yen, Z. Liu, M. Yu, H. Zhao, Z. Lu, G. Li, H. Gao, Z. Liu, Z. Bao, X. Chen, *Nature.* **2023**, *614*, 456.
[9] N. Li, Y. Li, Z. Cheng, Y. Liu, Y. Dai, S. Kang, S. Li, N. Shan, S. Wai, A. Ziaja, Y. Wang, J. Strzalka, W. Liu, C. Zhang, X. Gu, J. A. Hubbell, B. Tian, S. Wang, *Science.* **2023**, *381*, 686.
[10] Y. Sun, S. Shen, W. Deng, G. Tian, D. Xiong, H. Zhang, T. Yang, S. Wang, J. Chen, W. Yang, *Nano Energy.* **2023**, *105*, 108024.
[11] Y. Xu, S. Yu, L. Liu, W. Lin, Z. Cao, Y. Hu, J. Duan, Z. Huang, C. Wei, Z. Guo, T. Wu, Z. Chen, Q. Liao, Y. Zheng, X. Liao, *Adv. Funct. Mater.* **2024**, *34*, 2411331.
[12] G. Tian, W. Deng, T. Yang, J. Zhang, T. Xu, D. Xiong, B. Lan, S. Wang, Y. Sun, Y. Ao, L. Huang, Y. Liu, X. Li, L. Jin, W. Yang, *Adv. Mater.* **2024**, *36*, 2313612.
[13] D. Won, H. Kim, J. Kim, H. Kim, M. W. Kim, J. Ahn, K. Min, Y. Lee, S. Hong, J. Choi, C.-Y. Kim, T.-S. Kim, S. H. Ko, *Nat. Electron.* **2024**, *7*, 475.
[14] W. Heng, S. Solomon, W. Gao, *Adv. Mater.* **2022**, *34*, 2107902.

[15] C. B. Cooper, S. E. Root, L. Michalek, S. Wu, J. Lai, M. Khatib, S. T. Oyakhire, R. Zhao, J. Qin, Z. Bao, *Science.* **2023**, *380*, 935.
[16] Y. Liu, C. Yiu, Z. Song, Y. Huang, K. Yao, T. Wong, J. Zhou, L. Zhao, X. Huang, S. K. Nejad, M. Wu, D. Li, J. He, X. Guo, J. Yu, X. Feng, Z. Xie, X. Yu, *Sci. Adv.* **2022**, *8*, eabl6700.
[17] T. Yang, W. Deng, G. Tian, L. Deng, W. Zeng, Y. Wu, S. Wang, J. Zhang, B. Lan, Y. Sun, L. Jin, W. Yang, *Mater. Horiz.* **2023**, *10*, 5045.
[18] B. Lan, X. Xiao, A. D. Carlo, W. Deng, T. Yang, L. Jin, G. Tian, Y. Ao, W. Yang, J. Chen, *Adv. Funct. Mater.* **2022**, *32*, 2207393.
[19] S. Wang, W. Deng, T. Yang, Y. Ao, H. Zhang, G. Tian, L. Deng, H. Huang, J. Huang, B. Lan, W. Yang, *Adv. Funct. Mater.* **2023**, *33*, 2214503.
[20] M. Biao, H. Ke, C. Gangsheng, T. Yingnan, J. Nan, Z. Chao, L. Hong, *Soft Sci.* **2024**, *4*, 8.
[21] S. Yu, Y. Xu, Z. Cao, Z. Huang, H. Wang, Z. Yan, C. Wei, Z. Guo, Z. Chen, Y. Zheng, Q. Liao, X. Liao, Y. Zhang, *Adv. Funct. Mater.* **2024**, https://doi.org/10.1002/adfm.202416984.
[22] Y. Li, X. Wei, Z. Liu, H. Kang, W. Han, *ACS Appl. Nano Mater.* **2024**, *7*, 8813.
[23] J. Chen, T. Song, X. Wang, Y. Zhou, T. Wang, X. Zhang, Y. Zhao, B. Yang, Y. Zhang, J. Chen, K. Chen, Y. Li, W. Han, *Nano Energy.* **2024**, *131*, 110285.
[24] L. Zhang, L. Chen, S. Wang, S. Wang, D. Wang, L. Yu, X. Xu, H. Liu, C. Chen, *Nat. Commun.* **2024**, *15*, 3859.
[25] T. Lei, J. Pan, N. Wang, Z. Xia, Q. Zhang, J. Fan, L. Tao, W. Shou, Y. Gao, *Mater. Horiz.* **2024**, *11*, 1234.
[26] X. Guan, B. Zhang, Y. Zhu, X. Sun, K. Meng, Z. Wang, A. H. El-Gowily, Y. Chen, S. Zheng, Q. Han, M. S. Elafify, M. An, P. Rao, M. Ueda, Y. Ito, *Adv. Funct. Mater.* **2024**, *34*, 2313633.
[27] W. Zhao, Z. Lin, Z. Sun, Z. Zhu, W. Lin, Y. Xu, Z. Peng, Z. Sun, Z. Wang, *Adv. Sci.* **2023**, *10*, 2303338.
[28] C. C. Kim, H. H. Lee, K. H. Oh, J. Y. Sun, *Science.* **2016**, *353*, 682.
[29] N. Bai, Y. Xue, S. Chen, L. Shi, J. Shi, Y. Zhang, X. Hou, Y. Cheng, K. Huang, W. Wang, J. Zhang, Y. Liu, C. F. Guo, *Nat. Commun.* **2023**, *14*, 7121.
[30] E. K. Boahen, B. Pan, H. Kweon, J. S. Kim, H. Choi, Z. Kong, D. J. Kim, J. Zhu, W. B. Ying, K. J. Lee, D. H. Kim, *Nat. Commun.* **2022**, *13*, 7699.
[31] Z. Wenchao, Z. Haifeng, L. Wenkang, C. Manlin, Z. Min, Z. Long, *Nano-Micro Lett.* **2024**, *16*, 99.
[32] J. Shi, Y. Dai, Y. Cheng, S. Xie, G. Li, Y. Liu, J. Wang, R. Zhang, N. Bai, M. Cai, Y. Zhang, Y. Zhan, Z. Zhang, C. Yu, C. F. Guo, *Sci. Adv.* **2023**, *9*, eadf8831.
[33] H. Song, G. Luo, Z. Ji, R. Bo, Z. Xue, D. Yan, F. Zhang, K. Bai, J. Liu, X. Cheng, W. Pang, Z. Shen, Y. Zhang, *Sci. Adv.* **2022**, *8*, eabm3785.
[34] Y. Li, Z. Tian, X. Gao, H. Zhao, X. Li, Z. Wang, Z. Yu, D. Yang, *Adv. Funct. Mater.* **2023**, *33*, 2308845.
[35] H. Lei, J. Zhao, X. Ma, H. Li, D. Fan, *Adv. Healthcare Mater.* **2021**, *10*, 2101089.
[36] H. Ding, Z. Xin, Y. Yang, Y. Luo, K. Xia, B. Wang, Y. Sun, J. Wang, Y. Zhang, H. Wu, S. Fan, L. Zhang, K. Liu, *Adv. Funct. Mater.* **2020**, *30*, 1909616.
[37] Y. Dobashi, D. Yao, Y. Petel, T. N. Nguyen, M. S. Sarwar, Y. Thabet, C. L. W. Ng, E. S. Glitz, G. T. M. Nguyen, C. Plesse, F. Vidal, C. A. Michal, J. D. W. Madden, *Science.* **2022**, *376*, 502.
[38] Z. Wang, T. Li, Y. Chen, J. Li, X. Ma, J. Yin, X. Jiang, *Nat. Commun.* **2022**, *13*, 6487.
[39] A. Chortos, *Cell.* **2022**, *185*, 2653.
[40] S. Xu, J.-X. Yu, H. Guo, S. Tian, Y. Long, J. Yang, L. Zhang, *Nat. Commun.* **2023**, *14*, 219.
[41] H. J. Yoon, D. M. Lee, Y. J. Kim, S. Jeon, J. H. Jung, S. S. Kwak, J. Kim, S. Kim, Y. Kim, S. W. Kim, *Adv. Funct. Mater.* **2021**, *31*, 2100649.
[42] X. Pan, Q. Wang, D. Benetti, Y. Ni, F. Rosei, *Nano Energy.* **2022**, *103*, 107718.
[43] M. N. Biutty, J. M. Koo, J. H. Kim, S. Kim, U. H. Choi, K. B. C. Imani, J. Yoon, B. Y. Chang, S. I. Yoo, *J. Mater. Chem. A.* **2022**, *10*, 11881.
[44] Y. Liu, Y. Hu, J. Zhao, G. Wu, X. Tao, W. Chen, *Small.* **2016**, *12*, 5074.
[45] J. Zhao, S. Han, Y. Yang, R. Fu, Y. Ming, C. Lu, H. Liu, H. Gu, W. Chen, *ACS Nano.* **2017**, *11*, 8590.
[46] C. Lu, X. Liao, D. Fang, X. Chen, *Nano Lett.* **2021**, *21*, 5369.
[47] C. Lu, X. Chen, *Chem. Phys. Lett.* **2022**, *803*, 139872.
[48] D. S. Liu, H. Ryu, U. Khan, C. Wu, J. H. Jung, J. Wu, Z. Wang, S. W. Kim, *Nano Energy.* **2021**, *81*, 105610.
[49] K. Y. Chun, Y. J. Son, E. S. Jeon, S. Lee, C. S. Han, *Adv. Mater.* **2018**, *30*, 1706299.
[50] Y. He, J. Wu, M. Lin, S. Xiao, H. Liu, P. Zhou, *J. Mater. Chem.C.* **2021**, *9*, 16378.
[51] J. I. Lee, H. Choi, S. H. Kong, S. Park, D. Park, J. S. Kim, S. H. Kwon, J. Kim, S. H. Choi, S. G. Lee, D. H. Kim, M. S. Kang, *Adv. Mater.* **2021**, *33*, 2100321.
[52] J. Odent, N. Baleine, V. Biard, Y. Dobashi, C. Vancaeyzeele, G. T. M. Nguyen, J. D. W. Madden, C. Plesse, J.-M. Raquez, *Adv. Funct. Mater.* **2023**, *33*, 2210485.
[53] V. Asmita, N. Hnin Yin Yin, I. M. Hsing, *Mater. Futures.* **2024**, *3*, 033501.
[54] C. F. Guimarães, L. Gasperini, A. P. Marques, R. L. Reis, *Nat. Rev. Mater.* **2020**, *5*, 351.
[55] Z. Li, X. Li, S. He, Z. Zhou, L. Liu, W. Yu, X. Zhao, *Acta Phys. Sin.* **2022**, *71*, 137801.
[56] L. Chen, Z. Jin, W. Feng, L. Sun, H. Xu, C. Wang, *Science.* **2024**, *383*, 1455.
[57] V. Kapur, J. Charkoudian, J. L. Anderson, *J. Membr. Sci.* **1997**, *131*, 143.
[58] J. Peng, D. Cao, Z. He, J. Guo, P. Hapala, R. Ma, B. Cheng, J. Chen, W. J. Xie, X. Z. Li, P. Jelínek, L. M. Xu, Y. Q. Gao, E. G. Wang, Y. Jiang, *Nature.* **2018**, *557*, 701.